Available online at www.sciencedirect.com
SCIENCE DIRECT®
Journal of Computational Physics 193 (2004) 666–696
JOURNAL OF COMPUTATIONAL PHYSICS
www.elsevier.com/locate/jcp

Construction of local boundary conditions for an eigenvalue problem using micro-local analysis: application to optical waveguide problems

Hélène Barucq [a], Chokri Bekkey [b], Rabia Djellouli [c,*]

[a] *Laboratoire de Mathématiques Appliquées, Université de Pau et des Pays de l'Adour, IPRA – Avenue de l'Université, BP 1155, Pau Cedex 64013, France*
[b] *Laboratoire d'Ingénierie Mathématique, Ecole Polytechnique de Tunisie, EPT, BP 743, La Marsa 2070, Tunisia*
[c] *Department of Aerospace Engineering Sciences and Center for Aerospace Structures, University of Colorado at Boulder, Boulder, CO 80309-0429, USA*

Received 25 March 2002; received in revised form 17 March 2003; accepted 16 July 2003

Abstract

We present a general procedure based on the pseudo-differential calculus for deriving artificial boundary conditions for an eigenvalue problem that characterizes the propagation of guided modes in optical waveguides. This new approach allows the construction of local conditions that (a) are independent of the frequency regime, (b) preserve the sparsity pattern of the finite element discretization, and (c) are applicable to arbitrarily shaped convex artificial boundaries. The last feature has the potential for reducing the size of the computational domain. Numerical results are presented to highlight the potential of conditions of order 1/2 and 1, for improving significantly the computational efficiency of finite element methods for the solution of optical waveguide problems.

Keywords: Generalized eigenvalue problem; Micro-local analysis; Artificial boundary conditions; Optical fibre; Guided mode; Weak guidance; Finite element method; IRAM

1. Introduction

The problem of the propagation of guided modes in optical fibres can be formulated, under the weak guidance assumptions, as an eigenvalue scalar problem set in the whole plane $\mathbb{R}^2$ [6,18,20,25,30]. Therefore, discretizing this eigenvalue problem by the finite element method requires first defining a bounded computational domain. This is typically achieved by surrounding the core of the considered fibre by an artificial

* Corresponding author. Present address: Department of Mathematics, California State University Northridge, 18111 Nordhoff Street, Northridge, 91330-8313, USA. Tel.: +1-818-677-5867; fax: +1-818-677-2721.
E-mail address: Rabia.Djellouli@csun.edu (R. Djellouli).

0021-9991/$ - see front matter
doi:10.1016/j.jcp.2003.07.037

exterior boundary positioned at some distance from the interface core–cladding. This distance is usually measured in multiples of the wavelength of interest. The behavior of the guided field is then represented by a boundary condition specified on the artificial boundary. The idea here is (a) to "prohibit" the reflection of waves from the artificial boundary to avoid spurious solutions, and (b) to define an effective computational domain, the region that is inside the artificial boundary, that is as "small" as possible to be cost-effective.

Many attempts have been made so far to achieve this important objective with however limited success (see [7,16,32] among others). For an overview about the performance of such approaches, one may see the introduction in [11] and also [13,14,29]. Most recently, the last two authors and their co-workers suggested a new artificial boundary condition of Robin-type that couples the propagation constants to their corresponding fields [11]. The resulting formulation of the optical waveguide problem in a finite domain allowed the computation of dispersion curves with an excellent level of accuracy according to the numerical results reported in [11]. The main drawback of this new formulation is that the proposed boundary condition requires that the artificial boundary to be circular. This restriction on the geometry of the artificial boundary often leads to a larger than needed computational domain, which hampers computational efficiency.

Our objective in this paper is to generalize the boundary condition suggested in [11] by constructing local artificial boundary conditions that can operate on arbitrarily shaped artificial boundaries (and then circumscribe more closely the interface core–cladding of the considered fibre) and to assess their computational efficiency. The procedure we propose here for deriving such boundary conditions is based on the approximation of the Dirichlet to Neumann operator (D_tN) by using the pseudo-differential calculus (see Section 4.1). A similar technique has been suggested in [2], in the case of Helmholtz equation, to extend the second order Bayliss–Gunzburger–Turkel boundary condition [4] in order to accommodate boundaries of arbitrary shape. However, the technique proposed in [2] is based on a high frequency regime assumption at the so-called *localization step* (see Section 4.1.2), and therefore cannot be applied to the considered eigenvalue problem since it requires that the propagation constants (the eigenvalues) must be very large. Such assumption is not valid for optical waveguide problems because, in practice, the propagation constants may be very small. Our approach does not require such restriction at the localization step and therefore its domain of validation is independent of the frequency band. We point out that, while in principle the proposed procedure can derive boundary conditions of any order in the sense of Definition 1 (see Section 4.1.2), the conditions of practical interest, from both mathematical and numerical point of view, are in fact of order 1/2 and 1 only (see Section 3). Indeed, from the mathematical point of view, the spectral analysis of the resulting eigenvalue problem, set in the bounded domain delimited by the artificial boundary, can be performed by applying the classical self-adjoint operators theory [22]. We have accomplished such analysis in Section 4.2 and have showed that the corresponding solutions have the same properties as the solutions of the original problem (the eigenvalue problem set in $\mathbb{R}^2$). From the numerical point of view, these two conditions are (a) easy to implement in any finite element code since they requires only additional mass-like matrices on the artificial boundary (see Section 5.1), and (b) more versatile than the boundary condition suggested in [11] because they are applicable to any convex geometry of the artificial boundary. Consequently, for non-circular-shaped cores, it is expected that these conditions allow smaller computational domains and then, lead to better computational efficiencies. We present in Section 5.2 several numerical results to highlight their potential for reducing the size of the computational domain while maintaining the level of accuracy reached by the condition suggested in [11].

2. Preliminaries

First, we describe the class of optical waveguides we focus on throughout this paper. Then, we recall the mathematical formulation that characterizes the propagation of guided modes of such structures.

2.1. Physical model

We recall that an optical fibre is a cylindrical dielectric structure assumed to be infinitely extended along its axis denoted by Ox_3 that is called the propagation's axis (Fig. 1). In the transverse direction x_1 and x_2, an optical fibre is constituted of two regions: a core and a cladding (Fig. 1). The open bounded subset Ω of $\mathbb{R}^2$ represents the fibre's core. The cladding, denoted by Ω^e, is the domain that surrounds Ω and is assumed to be infinite, i.e., $\Omega^e = \mathbb{R}^2 \setminus \overline{\Omega}$. This is a classical assumption since the guided modes' fields decrease exponentially to zero out of the core of the fibre and the size of the cladding is typically hundred times larger than the size of the core [18,20]. Furthermore, these regions are completely determined once we know the profile of the refractive index n of the considered fibre. The refractive index n is a real valued function depending on $x = (x_1, x_2)$ and satisfying $n \in L^\infty(\mathbb{R}^2)$ with $\inf_{x\in\mathbb{R}^2} n(x) = n_- > 0$. In addition, we assume throughout this paper that all the optical fibres have a *homogeneous* cladding. This means that the refractive index is constant outside the core, i.e.,

$$n(x) = n_\infty \quad \forall x \in \Omega^e = \mathbb{R}^2 \setminus \overline{\Omega}. \tag{1}$$

Moreover, in order to ensure the propagation of guided modes, we assume as in [6,18] that the refractive index satisfies

$$n_+ > n_\infty, \tag{2}$$

where

$$n_+ = \sup_{x\in\mathbb{R}^2} n(x).$$

2.2. Problem statement: the eigenvalue problem

We consider, in this work, the guided modes propagation under the weak guidance assumptions. This means that the refractive index variations are *small* compared to the wavenumber k. Under these assumptions, the longitudinal component of the electromagnetic field is neglected. Therefore, the Maxwell system is decoupled and any transverse component of the electromagnetic field u and its corresponding propagation constant β satisfy the following eigenvalue problem [18,25,30]:

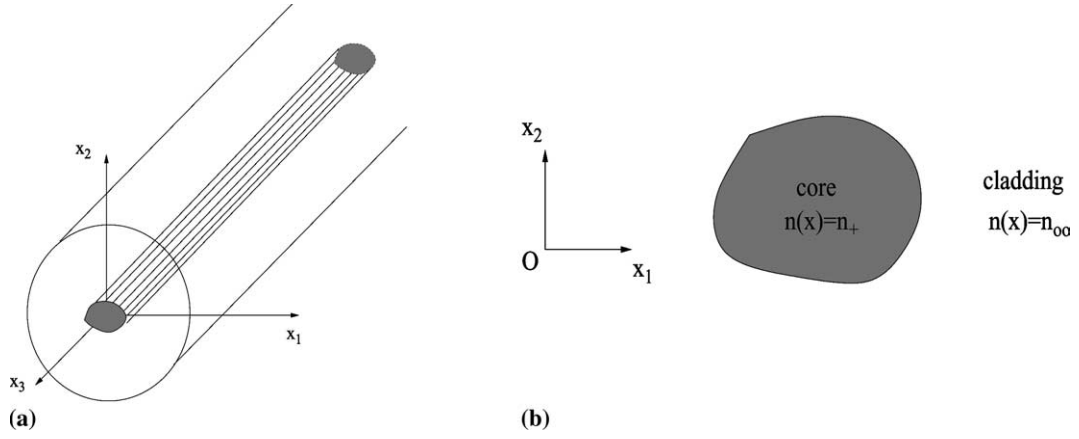

Fig. 1. (a) An optical fibre. (b) Transverse section of an optical fibre.

$$\text{(EVP)}\quad \text{Find } \lambda \in]0, V^2[\text{ and } u \in H^1(\mathbb{R}^2);\ u \neq 0 \text{ such that } -\Delta u + q(x)u = -\lambda u \text{ in } \mathbb{R}^2, \tag{3}$$

where

$$\lambda = \beta^2 - k^2 n_\infty^2, \tag{4}$$

$$V^2 = k^2\left(n_+^2 - n_\infty^2\right), \tag{5}$$

$$q(x) = -k^2\left(n^2 - n_\infty^2\right) \tag{6}$$

and where k is the wavenumber ($k > 0$).

For more details on the derivation and the physical background of EVP, we invite the reader to see, for example [30, pp. 403–407 and Appendix].

Note that q is a bounded function with a compact support included in the fibre's core Ω. λ (resp., u) is an eigenvalue (resp., its associated eigenfunction) of EVP. Hence, determining the guided modes that propagate, under the weak guidance assumptions, in the considered optical fibre, requires solving the eigenvalue problem EVP that is set in the whole plane $\mathbb{R}^2$.

EVP has been thoroughly investigated and a considerable amount of mathematical results pertaining to existence, number, and dependence with respect to opto-geometrical parameters of guided modes can be found in [6,8,18,25,30], among other references.

3. Announcement of the main results

The application of a finite element technique to the solution of the eigenvalue problem EVP requires first the definition of a bounded computational domain. This is typically achieved by surrounding the given core of the fibre by an artificial boundary Σ at some distance, that is usually measured in multiple of the wavelength of interest, from the interface core–cladding Γ. Then, a boundary condition that prohibits the reflection of the guided waves from the artificial boundary is specified on Σ.

Our aim in this work is to propose the following new formulation of EVP in a bounded domain, where Σ can be an arbitrarily shaped convex artificial boundary (see Fig. 2):

$$\text{(BVP)}\quad \text{Find } \lambda_\Sigma \in]0, V^2[\text{ and } u_\Sigma \in H^1(\Omega_\Sigma);\ u_\Sigma \neq 0 \text{ such that}$$

$$\text{(BVP)}\quad -\Delta u_\Sigma + q(x)u_\Sigma = -\lambda_\Sigma u_\Sigma \quad \text{in } \Omega_\Sigma, \tag{7}$$

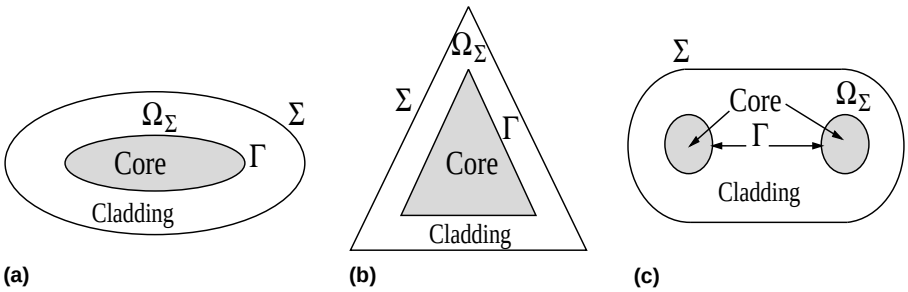

Fig. 2. Examples of optical fibres surrounded by artificial boundaries. (a) An elliptical-shaped artificial boundary. (b) An triangular-shaped artificial boundary. (c) An cigar-shaped artificial boundary.

$$(\mathrm{BVP}) \quad \frac{\partial u_\Sigma}{\partial v} + M_m(\lambda_\Sigma) u_\Sigma = 0 \quad \text{on } \Sigma, \tag{8}$$

Ω_Σ is a bounded domain, with Σ as its outer boundary. We place Σ in such a way that Ω_Σ contains the core of the considered fibre (Fig. 2), and hence the support of the function $q \in L^\infty(\mathbb{R}^2)$. $\vec{v}$ denotes the outward directed unitary normal vector. Besides, we assume that the artificial boundary Σ is at least Lipschitzian. Finally, the trace operator $M_m(\lambda_\Sigma)$ $(m = 1, 2)$ is defined as follows:

$$M_1(\lambda_\Sigma) = \sqrt{\lambda}\mathbb{I} \tag{9}$$

and

$$M_2(\lambda_\Sigma) = \left(\sqrt{\lambda} + \frac{\mathscr{K}}{2}\right)\mathbb{I}, \tag{10}$$

$\mathscr{K}$ denotes the curvature of the considered artificial boundary Σ [12] and $\mathbb{I}$ the identity mapping.

The following four observations are noteworthy:

- First, the Fourier–Robin type condition (8) is not an exact condition. It is, in fact, an approximation of the D_tN (the Dirichlet to Neumann) operator. Indeed, since the D_tN operator is a pseudo-differential operator of order +1 [28], we can apply Nirenberg's decomposition theorem and derive a Taylor expansion of this operator [19]. We propose later (cf. Section 4.1) a new procedure to approximate such a series and prove that the constructed conditions (8 and 9) (resp., (8 and 10)) is an approximation of order 1/2 (resp., 1). We point out that it is also possible to use this procedure for constructing conditions of higher order. However, these higher order conditions are not of practical interest because their expressions contain the eigenvalue λ_Σ with negative powers [3].
- Second, in the case where Σ is a circle, the condition (8 and 9) is identical to the one proposed in [11]. However, the requirement of a circular-shaped artificial boundary Σ often leads to a larger than needed computational domain, which hampers computational efficiency. Hence, this new condition is more versatile than the previous one [11] since it is applicable to an arbitrarily shaped but convex artificial boundary and then, it has the potential for reducing the size of the computational domain.
- Third, since the exterior boundary condition (8) associated with either Eq. (9) or Eq. (10) is not an exact condition, BVP is not equivalent to EVP in the sense that, the restriction to the bounded domain Ω_Σ of exact eigenfunctions are a priori not solutions of BVP. This is not the case when an exact condition such as the D_tN operator is applied on a circular exterior boundary [7]. Nevertheless, applying the spectral theory of self-adjoint operators to BVP (see Section 4.2) shows that the solutions of BVP have in fact the same properties (existence, finitude, continuous dependence with respect to the opto-geometrical parameters, etc.) as the exact guided modes solutions of EVP. Moreover, the numerical results we have reported in Section 5 indicate clearly that the exact guided modes solutions of EVP are approximated by the solutions of BVP with an excellent level of accuracy.
- Last, it is important to note that we have reduced the classical eigenvalue problem EVP defined in the whole domain $\mathbb{R}^2$ to the boundary value problem BVP defined in a bounded domain Ω_Σ but nonlinear with respect to the eigenvalues λ_Σ. Hence, the obtained problem is no longer a classical eigenvalue problem. However, since the corresponding variational formulation to BVP is given by

$$\begin{aligned} &\text{Find } \lambda_\Sigma \in]0, V^2[\text{ and } u_\Sigma \in H^1(\Omega_\Sigma);\ u_\Sigma \neq 0 \text{ such that } a_\Sigma(\lambda_\Sigma; u_\Sigma, v) = -\lambda_\Sigma \int_{\Omega_\Sigma} u_\Sigma v \,\mathrm{d}x; \\ &\forall v \in H^1(\Omega_\Sigma) \end{aligned} \tag{11}$$

where

$$a_\Sigma(\lambda_\Sigma; u_\Sigma, v) = \int_{\Omega_\Sigma} \nabla u_\Sigma \cdot \nabla v \, \mathrm{d}x + \int_{\Omega_\Sigma} q(x) u_\Sigma v \, \mathrm{d}x + \int_\Sigma M_m(\lambda_\Sigma) u_\Sigma v \, \mathrm{d}\sigma_x. \tag{12}$$

We will show later (see Section 5) that the nonlinearity of this new formulation does not represent – at least from a numerical point of view – a major difficulty to overcome. Indeed, the application of the finite element discretization to the variational formulation given by Eqs. (11) and (12) leads to solving a generalized eigenvalue problem, for which there exists a wide choice of numerical solution methods [15,23].

4. Mathematical analysis

In this section, we first present our procedure for deriving the boundary conditions that can operate on arbitrarily shaped artificial boundaries (see Eq. (8)). Then, we analyze the mathematical properties of the solutions of the obtained boundary value problem BVP.

The proposed approach for constructing non-reflecting boundary conditions distinguishes itself from existing methodology by (a) it does not require high frequency regime assumption and (b) it does not assume specific geometries (such as a circle) for the artificial boundary. Our approach assumes, however, that the artificial boundary needs to be (a) convex, which is not a restrictive condition for practical applications, and (b) located sufficiently far from the boundary Γ_1, of the smallest convex containing the cores of the considered waveguide. The numerical results we report in this paper tend to indicate that the artificial boundary is typically located at a fraction of a wavelength from Γ_1 in order to achieve an acceptable level of accuracy.

4.1. Construction of the boundary conditions

We present a general and rigorous procedure for constructing the boundary conditions (8). The idea is to approximate the D_tN operator using the pseudo-differential calculus. This approximation is performed in two steps. The first one consists in deriving a Taylor expansion of the D_tN operator by applying Nirenberg's decomposition theorem [19]. This classical expansion is called the *factorization* step of the approximation. The second one is the so-called *localization* step of the approximation. It consists in computing truncated sums of the obtained series and approximating the resulting operator by a differential operator under some geometrical assumptions on Σ that we will specify in Section 4.1.2. A similar technique has been already proposed by Antoine et al. [2] to derive radiation boundary conditions for the exterior Helmholtz equation. However, the technique developed in [2] is based on a high frequency regime assumption at the localization step. Hence, its application to optical waveguide problems is valid *only* for higher guided modes, i.e., the eigenvalues λ_Σ must be large which constitutes a severe limitation. Our approach does not require such an assumption and then allows to derive the boundary conditions (8) independently of the frequency band.

4.1.1. The factorization procedure

It is well known that in general the key element in constructing artificial boundary conditions is the mode selection which would guarantee the appropriate behavior of the field at the artificial boundary. Since the operator that we consider here is a Helmholtz-type equation, the idea we propose is to perform this mode selection by going back to the unsteady wave equation and identifying the appropriate modes based on their direction of propagation at the artificial boundary. This approach is not new and has been adopted by Antoine et al. [2] to derive non-reflecting boundary conditions for the Helmholtz equation.

We first consider Γ_1 the boundary of the smallest convex domain that contains the cores of the considered waveguide. We point out that if the core–cladding boundary Γ is convex, then $\Gamma = \Gamma_1$. Then, we

rewrite the Laplace operator in a system of local coordinates defined in the so-called tubular neighborhood of the core–cladding boundary Γ_1. This type of neighborhood can be parameterized as follows:

$$\Sigma_r = \{x \in \mathbb{R}^2 \,|\, x = p + r\vec{v}(p)\}, \tag{13}$$

where r is a non-negative fixed parameter, $p = p(s)$ is the orthogonal projection of x onto Γ_1, s is the curvilinear abscissa, and $\vec{v}$ is the outward unitary vector, normal to Γ_1. We note that Σ_r is parallel to Γ_1 and we have $\Sigma_0 = \Gamma_1$.

Hence, by setting

$$u(x) = \widetilde{u}(r, s) \tag{14}$$

and applying the chain rule, we deduce that the Laplace operator can be written in the coordinates (r, s) as follows:

$$\Delta u = \partial_r^2 \widetilde{u} + \mathscr{K}_r \widetilde{u} + h^{-1}\partial_s\left(h^{-1}\partial_s \widetilde{u}\right), \tag{15}$$

where $\mathscr{K}_r$ is the curvature of Σ_r obtained from the curvature $\mathscr{K}$ of Γ_1 as follows:

$$\mathscr{K}_r = \frac{\mathscr{K}}{1 + r\mathscr{K}} \tag{16}$$

and

$$h = 1 + r\mathscr{K}. \tag{17}$$

Next, we introduce the following intermediate function:

$$v(r, s, t) = \mathrm{e}^{\sqrt{\lambda}t}\widetilde{u}(r, s), \tag{18}$$

where t is a new variable that can be viewed as a time variable.

Since the couple (λ, u) is a solution of EVP, we deduce from Eqs. (15) and (18), that the function v satisfies

$$Pv = \partial_r^2 v + \mathscr{K}_r \partial_r v + h^{-1}\partial_s\left(h^{-1}\partial_s v\right) - \partial_t^2 v = 0. \tag{19}$$

We note that P is nothing but the wave operator. Hence, unlike the case of the Helmholtz equation [2], P is a hyperbolic operator. Therefore, the application of Nirenberg's decomposition theorem to P is straightforward [19]. Here, we briefly summarize the main steps of this factorization.

First, we introduce the dual variables (ω, ξ) of (t, s) so we can apply the Fourier transform to the operator P and compute its symbol $\mathscr{P}$. Hence, we have

$$\mathscr{P}(r, s, t, \xi, \omega) = \partial_r^2 + \mathscr{K}_r\partial_r + \mathrm{i}h^{-1}(\partial_s h^{-1})\xi - h^{-2}\xi^2 + \omega^2 = 0. \tag{20}$$

Therefore, there exists two classical pseudo-differential operators A^+ and A^- of order $+1$, depending smoothly on r, such that the operator P can be decomposed as follows:

$$P = (\partial_r + \mathrm{i}A^-)(\partial_r + \mathrm{i}A^+). \tag{21}$$

In addition, the uniqueness of this decomposition is insured by the following integral representation:

$$A^{\mp}v(r, s, t) = \int \mathrm{e}^{(\mathrm{i}\omega t + \xi s)} a^{\mp}(r, s, t, \xi, \omega)\hat{v}(r, \xi, \omega)\,\mathrm{d}\xi\,\mathrm{d}\omega, \tag{22}$$

where a^+ and a^- are, respectively, the symbols of A^+ and A^- [9]. $\hat{v}$ is the Fourier transform of v with respect to the variables of time and space (t,s). Moreover, it is well known that since A^+ and A^- are classical pseudo-differential operators in OPS^1 [27], their symbols can be expanded as follows:

$$a^{\mp} \simeq \sum_{j=-1}^{+\infty} a^{\mp}_{-j}, \tag{23}$$

where the equivalence in Eq. (23) is to be understood in the sense specified in [2]. $a^{\mp}_{-j}$ are continuous functions with respect to the variables (r,s,t) and are homogeneous functions of degree $-j$ with respect to the dual variables (ω,ξ).

On the other hand, similarly to [2], from Eqs. (20) and (21), one can verify that the operators A^+ and A^- satisfy

$$A^- + A^+ = -\mathrm{i}\mathscr{K}_r, \tag{24}$$

$$A^- A^+ - \mathrm{i}\mathrm{Op}(\partial_r a^+) = \partial_t^2 - h^{-1}\partial_s\left(h^{-1}\partial_s v\right), \tag{25}$$

where $\mathrm{Op}(\partial_r a^+)$ is the pseudo-differential operator which symbol is $\partial_r a^+$.

Moreover, the operators A^+ and A^- are uniquely obtained from the computation of their symbols a^+ and a^- [9,27]. Hence, we can express the system (24) and (25) in terms of the symbols as follows [27]:

$$a^- + a^+ = -\mathrm{i}\mathscr{K}_r, \tag{26}$$

$$\sum_{\alpha=0}^{+\infty} \frac{(-\mathrm{i})^\alpha}{\alpha!}\partial_\xi^\alpha a^- \partial_s^\alpha a^+ - \mathrm{i}\partial_r a^+ = -(\omega^2 - h^{-2}\xi^2) - \mathrm{i}h^{-1}\left(\partial_s h^{-1}\right)\xi. \tag{27}$$

Next, using the expansion (23), we identify in the system (26) and (27), the symbols with the same degree of homogeneity. This allows to derive a recursive formula to express all of the symbols a^+_{-j} from the first one a^+_1. More specifically, from Eqs. (23) and (26), we deduce that

$$a^-_{-j} + a^+_{-j} = \begin{cases} -\mathrm{i}\mathscr{K}_r & \text{if } j = 0, \\ 0 & \text{if } j \neq 0. \end{cases} \tag{28}$$

Therefore, the combination of Eqs. (27) and (28), completely determines the symbol a^+ and then the operator A^+. Indeed, each symbol a^+_{-j} can be computed from the previous as follows:

$$a^+_1 = (\omega^2 - h^{-2}\xi^2)^{1/2}, \tag{29}$$

$$a^+_0 = -\frac{\mathrm{i}}{2}\mathscr{K}_r + \frac{\mathrm{i}}{2a^+_1}h^{-1}\left(\partial_s h^{-1}\right)\xi + \frac{\mathrm{i}}{4(a^+_1)^2}\left(\partial_r h^{-2}\right)\xi^2 + \frac{\mathrm{i}}{4(a^+_1)^3}h^{-2}\left(\partial_s h^{-2}\right)\xi^3, \tag{30}$$

$$a^+_{-j} = \frac{1}{2a^+_1}\left(\sum_{\substack{l+k=j-1 \\ l\geqslant 0, k\geqslant 0}} a^-_{-l}a^+_{-k} + \sum_{\alpha=1}^{j+1}\frac{(-\mathrm{i})^\alpha}{\alpha!}\sum_{\substack{l+k=j-1-\alpha \\ l\geqslant -1, k\geqslant -1}} \partial_\xi^\alpha a^-_{-l}\partial_s^\alpha a^+_{-k} - \mathrm{i}\partial_r a^+_{-j+1}\right); \quad j > 1. \tag{31}$$

We note that the expansion of each symbol $a^+_{-j}; j \geqslant 0$ depends on a^+_1, which in turn depends on the domain of the dual variables (ω,ξ).

By setting

$$\Psi(r) = \omega^2 - h^{-2}\xi^2 \tag{32}$$

it follows from Eq. (17) that

$$\Psi'(r) = 2h^{-3}\mathscr{K}_r\xi^2. \tag{33}$$

Since the artificial boundary Σ is assumed to be convex, its curvature $\mathscr{K}_r$ is then positive. Therefore, we deduce that $\Psi(r)$ is a non-decreasing function and has the sign of

$$\Psi(0) = \omega^2 - \xi^2. \tag{34}$$

Since the dual variables (ω, ξ) are in the cone of propagation corresponding to the hyperbolic region where outgoing and ingoing waves propagate [17], and since we are interested only in outgoing waves, we have

$$\Psi(0) > 0. \tag{35}$$

Therefore

$$\Psi(r) = \omega^2 - h^{-2}\xi^2 > 0. \tag{36}$$

Hence, a^+_{-j} is a real number and the solutions of EVP satisfy (in the micro-local sense)

$$\partial_r v + \mathrm{i}A^+ v = 0 \quad \text{on } \Sigma_r. \tag{37}$$

So far, we are in principle able to compute all symbols from the system (29)–(31) and to deduce uniquely the operator A^+. In practice, only few of them are really computed. Therefore, the operator A^+ is approximated by an operator A^+_m which symbol σ^{-m} is given by

$$\sigma^{-m} = \sum_{j=-1}^{m} a^+_{-j} \tag{38}$$

for a fixed $m \geqslant -1$. Then, A^+_m is a pseudo-differential operator in OPS^1 and $(A^+ - A^+_m) \in \mathrm{OPS}^{-(m+1)}$ [27].

In summary, by approximating the D_tN operator via the factorization of its symbol, we have derived a family of boundary conditions defined by

$$\partial_r v + \mathrm{i}A^+_m v = 0 \quad \text{on } \Sigma_r. \tag{39}$$

Unfortunately, this result is – at this step – not of practical interest because A^+_m is a non-local operator.

Next, we propose a procedure to *localize* the operator A^+_m in order to obtain local boundary conditions that are easy to implement in any finite element code. The localization process we suggest consists basically in *approximating* the pseudo-differential operator A^+_m by a differential operator under some geometrical assumptions that we will specify in the following section.

4.1.2. The localization process

The objective in this section is to approximate the global boundary condition given by Eq. (39) to construct local artificial boundary conditions that preserve the sparsity pattern of the finite element discretization. To do this, we assume that $r\mathscr{K}$ is *large* enough and then perform the Taylor expansion of the symbol σ^{-m} of A^+_m with respect to the inverse of $r\mathscr{K}$. This geometrical assumption means that the artificial boundary Σ_r is located very far away from the interface core–cladding Γ_1 as well as Σ_r and Γ_1 have a similar curvature.

In order to derive the Taylor expansion of the symbol σ^{-m} with respect to $1/r\mathscr{K}$, we compute first the Taylor expansion of the symbols a^+_{-j} $(j \geqslant -1)$.

4.1.2.1. Taylor expansion of the symbol a^+_1. First, we rewrite Eqs. (17) and (29) as follows:

$$a^+_1 = \omega\left(1 - \frac{h^{-2}\xi^2}{\omega^2}\right)^{1/2}, \tag{40}$$

$$h^{-2}(r,s) = \frac{1}{r^2\mathscr{K}^2}\left(1 + \frac{1}{r\mathscr{K}}\right)^{-2}. \tag{41}$$

Therefore, we deduce from Eq. (41) that

$$h^{-2}(r,s) = \frac{1}{r^2\mathscr{K}^2}\left(1 - \frac{2}{r\mathscr{K}} + \frac{1}{r\mathscr{K}}\varepsilon\left(\frac{1}{r\mathscr{K}}\right)\right), \tag{42}$$

where the real function ε satisfies

$$\lim_{\tau\to 0}\varepsilon(\tau) = 0. \tag{43}$$

Hence, from Eqs. (40) and (42), we deduce that a Taylor expansion of the first symbol a^+_1 is given by

$$a^+_1 = \omega - \frac{\xi^2}{2\omega}\frac{1}{r^2\mathscr{K}^2} + \frac{3\xi^2}{2\omega}\frac{1}{r^3\mathscr{K}^3} + \frac{1}{r^3\mathscr{K}^3}\varepsilon\left(\frac{1}{r\mathscr{K}}\right). \tag{44}$$

4.1.2.2. Taylor expansion of the symbol a^+_0. The derivation of such expansion requires the following intermediate results:

- From Eq. (16), we have

$$\mathscr{K}_r = \frac{1}{r}\left(1 + \frac{1}{r\mathscr{K}}\right)^{-1}. \tag{45}$$

  Therefore, we deduce that

$$\mathscr{K}_r = \frac{1}{r}\left(1 - \frac{1}{r\mathscr{K}} + \frac{1}{r^2\mathscr{K}^2} + \frac{1}{r^2\mathscr{K}^2}\varepsilon\left(\frac{1}{r\mathscr{K}}\right)\right). \tag{46}$$

- From Eq. (17), we deduce that

$$h^{-1}\partial_s h^{-1} = -h^{-3}r\mathscr{K}'(s). \tag{47}$$

  Using again Eq. (17), we rewrite Eq. (47) as follows:

$$h^{-1}\partial_s h^{-1} = -r\mathscr{K}'(s)\frac{1}{r^3\mathscr{K}^3}\left(1 + \frac{1}{r\mathscr{K}}\right)^{-3}. \tag{48}$$

  Therefore, we deduce that

$$h^{-1}\partial_s h^{-1} = \frac{1}{\mathscr{K}}\left(\frac{-\mathscr{K}'(s)}{r^2\mathscr{K}^2} + \frac{3\mathscr{K}'(s)}{r^3\mathscr{K}^3} + \frac{1}{r^3\mathscr{K}^3}\varepsilon\left(\frac{1}{r\mathscr{K}}\right)\right). \tag{49}$$

- From Eqs. (40) and (42), it follows that

$$\frac{1}{a_1^+} = \frac{1}{\omega}\left(1 - \frac{\xi^2}{\omega^2}\left(\frac{1}{r^2\mathscr{K}^2} - \frac{3}{r^3\mathscr{K}^3} + \frac{1}{r^3\mathscr{K}^3}\varepsilon\left(\frac{1}{r\mathscr{K}}\right)\right)\right)^{-1/2}. \tag{50}$$

Then,

$$\frac{1}{a_1^+} = \frac{1}{\omega} + \frac{\xi^2}{2\omega^3}\frac{1}{r^2\mathscr{K}^2} - \frac{3\xi^2}{2\omega^2}\frac{1}{r^3\mathscr{K}^3} + \frac{1}{r^3\mathscr{K}^3}\varepsilon\left(\frac{1}{r\mathscr{K}}\right). \tag{51}$$

Hence, we deduce from Eqs. (49) and (51) that

$$\frac{\mathrm{i}h^{-1}\partial_s h^{-1}}{2a_1^+} = \frac{-\mathrm{i}\mathscr{K}'(s)\xi}{2\mathscr{K}\omega}\frac{1}{r^2\mathscr{K}^2} + \frac{3\mathrm{i}\mathscr{K}'(s)\xi}{2\mathscr{K}\omega}\frac{1}{r^3\mathscr{K}^3} + \frac{1}{r^3\mathscr{K}^3}\varepsilon\left(\frac{1}{r\mathscr{K}}\right). \tag{52}$$

- From Eq. (50), we obtain

$$\frac{1}{(a_1^+)^2} = \frac{1}{\omega^2}\left(1 - \frac{\xi^2}{\omega^2}\left(\frac{1}{r^2\mathscr{K}^2} - \frac{3}{r^3\mathscr{K}^3} + \frac{1}{r^3\mathscr{K}^3}\varepsilon\left(\frac{1}{r\mathscr{K}}\right)\right)\right)^{-1}. \tag{53}$$

Therefore, we deduce that

$$\frac{1}{(a_1^+)^2} = \frac{1}{\omega^2} + \frac{\xi^2}{\omega^4}\frac{1}{r^2\mathscr{K}^2} - \frac{3\xi^2}{\omega^4}\frac{1}{r^3\mathscr{K}^3} + \frac{1}{r^3\mathscr{K}^3}\varepsilon\left(\frac{1}{r\mathscr{K}}\right). \tag{54}$$

Moreover, from Eq. (17), we deduce that

$$\partial_r h^{-2} = -2h^{-3}\mathscr{K}. \tag{55}$$

Besides, from Eq. (41), we deduce that

$$h^{-3} = \frac{1}{r^3\mathscr{K}^3} + \frac{1}{r^3\mathscr{K}^3}\varepsilon\left(\frac{1}{r\mathscr{K}}\right). \tag{56}$$

Therefore, it follows from Eqs. (54)–(56) that

$$\frac{\mathrm{i}\partial_r h^{-2}}{4(a_1^+)^2} = -\frac{\mathrm{i}\mathscr{K}}{2\omega^2}\frac{1}{r^3\mathscr{K}^3} + \frac{1}{r^3\mathscr{K}^3}\varepsilon\left(\frac{1}{r\mathscr{K}}\right). \tag{57}$$

- Finally, from Eq. (50), we have

$$\frac{1}{(a_1^+)^3} = \frac{1}{\omega^3}\left(1 - \frac{\xi^2}{\omega^2}\left(\frac{1}{r^2\mathscr{K}^2} - \frac{3}{r^3\mathscr{K}^3} + \frac{1}{r^3\mathscr{K}^3}\varepsilon\left(\frac{1}{r\mathscr{K}}\right)\right)\right)^{-3/2}. \tag{58}$$

Therefore, we deduce that

$$\frac{1}{(a_1^+)^3} = \frac{1}{\omega^3} + \frac{3\xi^2}{2\omega^5}\frac{1}{r^2\mathscr{K}^2} - \frac{15\xi^2}{6\omega^5}\frac{1}{r^3\mathscr{K}^3} + \frac{1}{r^3\mathscr{K}^3}\varepsilon\left(\frac{1}{r\mathscr{K}}\right). \tag{59}$$

Besides, from Eq. (17), we obtain that

$$h^{-2}\partial_s h^{-2} = -2r\mathscr{K}'(s)h^{-5}. \tag{60}$$

Therefore, using the Taylor expansion of h with respect to $1/r\mathscr{K}$, we deduce that

$$h^{-2}\partial_s h^{-2} = \frac{1}{r^4\mathscr{K}^4}\varepsilon\left(\frac{1}{r\mathscr{K}}\right). \tag{61}$$

Hence, it follows from Eqs. (59) and (61) that

$$\frac{h^{-2}\partial_s h^{-2}}{(a_1^+)^3} = \frac{1}{r^4\mathscr{K}^4}\varepsilon\left(\frac{1}{r\mathscr{K}}\right). \tag{62}$$

We are now ready to deduce the Taylor expansion of the symbol a_0^+ with respect to $1/r\mathscr{K}$. Indeed, from Eqs. (46), (49), (52), (57) and (62) one can verify that

$$\begin{aligned} a_0^+ = & -\frac{\mathrm{i}\mathscr{K}}{2}\frac{1}{r\mathscr{K}} + \left(\frac{\mathscr{K}}{2} - \frac{\mathrm{i}\mathscr{K}'}{2\mathscr{K}^2}\frac{\xi}{\omega}\right)\frac{1}{r^2\mathscr{K}^2} \\ & + \left(\frac{-\mathrm{i}\mathscr{K}}{2} + \frac{3\mathrm{i}\mathscr{K}'(s)}{2\mathscr{K}}\frac{\xi}{\omega} - \frac{\mathrm{i}\mathscr{K}}{2}\frac{\xi^2}{\omega^2}\right)\frac{1}{r^3\mathscr{K}^3} + \frac{1}{r^3\mathscr{K}^3}\varepsilon\left(\frac{1}{r\mathscr{K}}\right). \end{aligned} \tag{63}$$

4.1.2.3. Taylor expansion of the symbol a_{-j}^+; $j \geqslant 1$. A compact representation of such expansion is given by the following result:

Proposition 1. *For every $j \geqslant 1$ fixed, any Taylor expansion $T(a_{-j}^+)$ of the symbol a_{-j}^+ with respect to $1/r\mathscr{K}$ can be expressed as follows:*

$$T(a_{-j}^+) = \frac{1}{w^j}Q\left(\frac{1}{r\mathscr{K}}, \frac{\xi}{\omega}\right), \tag{64}$$

where Q is a polynomial of the variables $1/r\mathscr{K}$ and ξ/ω, which coefficients are continuous functions with respect to s.

Proof of Proposition 1. This result is an immediate consequence of the recursion relations given by Eqs. (29)–(31). Indeed, it is easy to verify that the symbol a_{-j}^+ can be written as follows:

$$a_{-j}^+ = (a_1^+)^{-j}Q_1\left(r, s; \frac{\xi}{a_1^+}\right), \quad j \geqslant -1, \tag{65}$$

where Q_1 satisfies

$$Q_1(r, s; X) = \sum_{0 \leqslant \alpha \leqslant d} c_\alpha(r, s)X^\alpha \tag{66}$$

and c_α are smooth functions with respect to r and s.

Therefore, Eq. (64) is deduced from Eqs. (44), (65) and (66).

At this point, it is important to observe in Eqs. (44) and (63) that the coefficients corresponding to $1/(r\mathscr{K})^l$; $l \geqslant 2$ depend on ω with negative powers and therefore give rise to boundary conditions depending on λ with negative powers. Hence, in order to derive boundary conditions of practical interest, we need to truncate the expression given by Eqs. (44) and (63) and only keep terms of order less or equal to 1 with respect to $1/r\mathscr{K}$. Moreover, when we compute σ^{-m} [see Eq. (38)], we also neglect the symbols a_{-j}^+; $j \geqslant 1$ since their expressions are proportional to $1/\omega^j$; $j \geqslant 1$ [see Eq. (64)].

Given that, we deduce the two following symbols σ^{-m} of practical interest

$$\sigma^1 = \omega \tag{67}$$

and

$$\sigma^0 = \omega - \frac{\mathrm{i}\mathscr{K}}{2}\frac{1}{r\mathscr{K}}. \tag{68}$$

Before retrieving the expression of the operator A_m^+ ($m = 0, 1$) from the symbol σ^{-m}, given by Eqs. (67) and (68), and in order to deduce the expression of the boundary conditions given by Eq. (39), we need to give a precise criterion for comparing the accuracy of each condition. Hence, similarly to [2], we introduce the following definition. □

Definition 1. We call a complete condition of order $\frac{m}{2}+1$, the condition

$$\partial_v u + \mathrm{Op}(\widetilde{\sigma}^{-m})u = 0 \quad \text{on } \Sigma_R, \tag{69}$$

where

$$\widetilde{\sigma}^{-m} = \sigma^{-m}|_{r=R}. \tag{70}$$

We are now ready to establish the following result

Theorem 1. *The condition of order* $1/2$ *is given by*

$$\partial_v u + \sqrt{\lambda}u = 0 \quad \text{on } \Sigma \tag{71}$$

and the condition of order 1 *is expressed as follows:*

$$\partial_v u + \sqrt{\lambda}u + \frac{\mathscr{K}_\Sigma}{2}u = 0 \quad \text{on } \Sigma, \tag{72}$$

where $\mathscr{K}_\Sigma$ *is the curvature of* Σ.

Proof of Theorem 1. We recall that our aim is to derive boundary conditions of the following form:

$$\partial_v v + \mathrm{i}A_m^+ v = 0, \tag{73}$$

where

$$v = \mathrm{e}^{\sqrt{\lambda}t}u(r,s). \tag{74}$$

First, let us assume that Σ is located at a distance $r = R$, i.e., $\Sigma = \Sigma_R$. At this distance, the symbols σ^1 and σ^0 are given by

$$\sigma^1|_{r=R} = \widetilde{\sigma}^1 = \omega, \tag{75}$$

$$\sigma^0|_{r=R} = \widetilde{\sigma}^0 = \omega - \frac{\mathrm{i}\mathscr{K}}{2}\frac{1}{R\mathscr{K}}. \tag{76}$$

Therefore, Eq. (73) can be written as follows:

$$\partial_v v|_{r=R} + \mathrm{Op}(\mathrm{i}\omega)v|_{r=R} = 0 \quad \text{for } m = -1 \tag{77}$$

and

$$\partial_v v|_{r=R} + \mathrm{Op}\left(\mathrm{i}\omega + \frac{\mathscr{K}}{2}\frac{1}{R\mathscr{K}}\right)v = 0 \quad \text{for } m = 0. \tag{78}$$

Since ω is the dual variable of t, we deduce from Eqs. (74) and (77) that

$$\partial_v u + \sqrt{\lambda}u = 0 \quad \text{on } \Sigma. \tag{79}$$

Similarly, from Eqs. (74) and (78), we have

$$\partial_v u + \left(\sqrt{\lambda} + \frac{1}{2R}\right)u = 0 \quad \text{on } \Sigma. \tag{80}$$

On the other hand, from Eq. (16) we note that $1/R$ is an approximation of the first order with respect to $1/R\mathscr{K}$ of the curvature $\mathscr{K}_\Sigma$ of Σ. Therefore, we modify Eq. (80) and set

$$\partial_v u + \left(\sqrt{\lambda} + \frac{\mathscr{K}_\Sigma}{2}\right)u = 0 \quad \text{on } \Sigma, \tag{81}$$

which achieves the Proof of Theorem 1. □

Remark 1. We point out that it is not of practical interest to construct in this case higher order boundary conditions. Indeed, the expression of such boundary conditions contain the eigenvalue λ_Σ with negative powers, as shown in [3]. Therefore, using these boundary conditions will lead to eigenvalue problems that are strongly nonlinear in terms of λ_Σ. Such eigenvalue problems might be extremely difficult to solve numerically.

4.2. Spectral analysis

We investigate now the mathematical properties of the solutions of BVP. Because of its nonlinearity, BVP is not well suited for carrying out such a study. However, since BVP resembles the eigenvalue problem analyzed in [11], we tailor the approach adopted in [11] to accomplish this investigation. Therefore, we carry out the spectral analysis of BVP in two steps. First, we introduce a family of classical eigenvalue problems and apply the spectral theory of self-adjoint operators [21,22]. Then, we solve a family of fixed-point problems using a classical argument of monotonicity in $\mathbb{R}$.

4.2.1. Classical eigenvalue problem

For a given parameter $\alpha \in]0, V^2[$, we introduce the following family of classical eigenvalue problems:

$(\widetilde{\mathbf{BVP}(\alpha)})$ Find $\mu_\Sigma(\alpha) \in \mathbb{R}$ and $u_{\Sigma,\alpha} \in H^1(\Omega_\Sigma)$; $u_{\Sigma,\alpha} \neq 0$ such that

$$(\widetilde{\mathbf{BVP}(\alpha)}) \quad -\Delta u_{\Sigma,\alpha} + \widetilde{q}(x)u_{\Sigma,\alpha} = \mu_\Sigma(\alpha)u_{\Sigma,\alpha} \quad \text{in } \Omega_\Sigma, \tag{82}$$

$$(\widetilde{\mathbf{BVP}(\alpha)}) \quad \frac{\partial}{\partial v}u_{\Sigma,\alpha} + f_s(\alpha)u_{\Sigma,\alpha} = 0 \quad \text{on } \Sigma, \tag{83}$$

where

$$\mu_\Sigma(\alpha) = k^2 n_+^2 - \beta_{\Sigma,\alpha}^2, \tag{84}$$

$$\widetilde{q}(x) = k^2\left(n_+^2 - n^2\right) \tag{85}$$

and f_s $(s = 1, 2)$ is a non-negative real function. The expression of f_s depends on the choice of the boundary operator M_s; $s = 1, 2$ [see Eqs. (9) and (10)]. More specifically, we have

$$f_s(\alpha) = \sqrt{V^2 - \alpha}; \quad \text{if } s = 1, \tag{86}$$

$$f_s(\alpha) = f_1(\alpha) + \frac{\mathscr{K}}{2}; \quad \text{if } s = 2. \tag{87}$$

Moreover, we associate to $\widetilde{\mathbf{BVP}}(\alpha)$ the following variational problem:

$(\widetilde{\mathbf{VBVP}}(\alpha))$ Find $\mu_\Sigma(\alpha) \in \mathbb{R}$ and $u_{\Sigma,\alpha} \in H^1(\Omega_\Sigma)$; $u_{\Sigma,\alpha} \neq 0$ such that

$$a_\Sigma(\alpha; u_{\Sigma,\alpha}, v) = \mu_\Sigma(\alpha) \int_{\Omega_\Sigma} u_{\Sigma,\alpha} v \, \mathrm{d}x \quad \forall v \in H^1(\Omega_\Sigma), \tag{88}$$

where $a_\Sigma(\alpha; \cdot, \cdot)$ is a bilinear form defined by

$$a_\Sigma(\alpha; v, w) = \int_{\Omega_\Sigma} \nabla v \cdot \nabla w \, \mathrm{d}x + \int_{\Omega_\Sigma} \widetilde{q}(x)\, vw \, \mathrm{d}x + \int_\Sigma f_s(\alpha)\, vw \, \mathrm{d}\sigma_\Sigma \quad \forall v, w \in H^1(\Omega_\Sigma). \tag{89}$$

It is then easy to verify that for a given $\alpha \in]0, V^2[$, the bilinear form $a_\Sigma(\alpha; \cdot, \cdot)$ is symmetric, continuous on $H^1(\Omega_\Sigma) \times H^1(\Omega_\Sigma)$. Moreover, since Σ is assumed to be convex, i.e., its curvature $\mathscr{K}_\Sigma$ is positive, then $a_\Sigma(\alpha; \cdot, \cdot)$ satisfies the following Gärding inequality.

For a given $\gamma_0 > 0$ there exists a positive constant $c(\gamma_0)$ such that

$$\forall \gamma \geqslant \gamma_0 \quad a_\Sigma(\alpha; v, v) + \gamma \|v\|^2_{L^2(\Omega_\Sigma)} \geqslant c(\gamma_0) \|v\|^2_{H^1(\Omega_\Sigma)} \quad \forall v \in H^1(\Omega_\Sigma). \tag{90}$$

Therefore, we are able to apply the spectral theory of self-adjoint operators [21,22] and to conclude that the eigenvalues of $\widetilde{\mathbf{BVP}}(\alpha)$ are positive, countable, with a finite multiplicity. Moreover, we characterize them via the Min–Max formula [10,21] as a sequence defined by

$$\mu^l_R(\alpha) = \operatorname*{Min}_{V_l \in \mathscr{V}_l} \operatorname*{Max}_{v \in V_l} \frac{a_R(\alpha; v, v)}{\|v\|^2_{L^2(\Omega_R)}}, \tag{91}$$

where

$$0 < \mu^1_\Sigma(\alpha) \leqslant \mu^2_\Sigma(\alpha) \leqslant \mu^3_\Sigma(\alpha) \leqslant \cdots \leqslant \mu^l_\Sigma(\alpha) \leqslant \cdots \tag{92}$$

and satisfying

$$\lim_{l \to +\infty} \mu^l_\Sigma(\alpha) = +\infty. \tag{93}$$

Moreover, similarly to [11], it is easy to verify that for l fixed, the function

$$\begin{aligned} &I =]0, V^2[\to \mathbb{R}^+, \\ &\alpha \mapsto \mu^l_\Sigma(\alpha) \end{aligned} \tag{94}$$

is non-increasing, continuous, and $\lim_{\alpha \to V^2} \mu^l_\Sigma(\alpha)$ exists and is finite.

4.2.2. Fixed-point problems

The solutions of BVP can be characterized as the solutions of the following family of fixed-point problems:

For $l \geqslant 1$ given,

$$(\mathrm{P}_\Sigma^l) \quad \text{Find } \alpha \in I =]0, V^2[\text{ such that } \mu_\Sigma^l(\alpha) = \alpha. \tag{95}$$

Because of the monotonicity and the continuity of the function $\alpha \to \mu_\Sigma^l(\alpha)$, we can apply the fixed-point theorem and conclude that, for l given, P_Σ^l has exactly one solution providing that $\lim_{\alpha \to V^2} \mu_\Sigma^l(\alpha) \leqslant V^2$. Therefore, the boundary value problem BVP admits at most a finite number of eigenvalues.

Finally, we prove in the following proposition that BVP admits at least one eigenvalue.

Proposition 2. *Assume that the refractive index n satisfies*

$$\int_{\mathbb{R}^2} \left(n^2 - n_\infty^2\right) \mathrm{d}x > 0. \tag{96}$$

Then, if the artificial boundary Σ is located far enough from the interface core–cladding Γ_1, BVP has at least one eigenvalue.

Proof of Proposition 2. In order to establish this proposition, we prove that P_Σ^1 admits a fixed-point μ_Σ^1. To do this, it suffices to establish that

$$\mu_\Sigma^1(\alpha) - V^2 < 0 \quad \forall \alpha \in]0, V^2[. \tag{97}$$

From Eqs. (88) and (91), we obtain

$$\mu_\Sigma^1(\alpha) - V^2 \leqslant \frac{a_\Sigma(\alpha; v, v) - V^2 \|v\|^2_{L^2(\Omega_\Sigma)}}{\|v\|^2_{L^2(\Omega_\Sigma)}} \quad \forall v \in H^1(\Omega_\Sigma). \tag{98}$$

Similarly to Proposition 3 in [11], we assume that Σ is far enough from Γ_1 such that there exists two positive real numbers a and R such that

$$\overline{\Omega} \subset B(0, a), \quad \overline{B(0, a)} \subset B(0, R) \quad \text{and} \quad \overline{B(0, R)} \subset \Omega_\Sigma. \tag{99}$$

We also introduce the following function:

$$v_R(x) = \begin{cases} 1 & \text{if } |x| \leqslant a, \\ \frac{\log(R) - \log|x|}{\log(R) - \log(a)} & \text{if } a \leqslant |x| \leqslant R, \\ 0 & \text{if } |x| \geqslant R. \end{cases} \tag{100}$$

It is easy to verify that $v_R \in H^1(\Omega_\Sigma) \cap H^1(\mathbb{R}^2)$ and

$$\|\nabla v_R\|_{L^2(\mathbb{R}^2)} \underset{R \to +\infty}{\to} 0. \tag{101}$$

Therefore, for R large enough, (97) is deduced from Eqs. (98) and (101). □

5. Numerical illustration

We illustrate in this section, by several numerical experiments, the potential of the use of boundary condition (8) associated with Eq. (10) applied on an artificial boundary Σ that is parallel to the interface core–cladding of the considered fibre, rather than the condition suggested in [11], for improving the computational efficiency of the finite element method applied to the solution of the waveguide problem BVP.

5.1. Discretization method and iterative solver

The variational problem (see Eqs. (11) and (12)) is approximated using a linear finite element method [21]. In practice, the computational domain Ω_Σ is decomposed into triangles, using a uniform mesh. We point out that in order to obtain an acceptable level of accuracy, the ratio λ/h, where λ is the wavelength and h is the discretization step, is chosen to be equal to 50 in all the numerical experiments reported in this paper. This choice is motivated by the grid convergence study performed by Djellouli et al. [11] (see Fig. 2 and Table 1). Therefore, the proposed boundary conditions (8), associated with either Eq. (9) or Eq. (10), introduces only additional (and standard) mass and stiffness matrices on Σ. The only issue that deserves special attention is the approximation of the curvature $\mathscr{K}$ of Σ, when Σ is an arbitrary convex boundary. To compute the curvature $\mathscr{K}$ of a chosen artificial boundary Σ in the context of the linear finite element approximation, we proceed as follows.

Let $T = (\mathscr{A}\mathscr{B}\mathscr{C})$ be a triangle which vertices $\mathscr{A}$, $\mathscr{B}$, and $\mathscr{C}$ belong to the artificial boundary Σ (Fig. 3), but are not necessarily connected to the same finite element. The curvature of Σ at point $\mathscr{B}$ can be approximated by the following formula [26]:

$$\mathscr{K}(\mathscr{B}) = \frac{4m(T)}{d_1 d_2 d_3}, \tag{102}$$

where $m(T)$ denotes the area of triangle T, and d_1, d_2, and d_3 the lengths of its edges (Fig. 3). The area $m(T)$ can be computed by any standard technique. However, if the angle at $\mathscr{B}$ is sufficiently close to π – that is if the triangle T is almost degenerate –, $m(T)$ is better evaluated as follows [26]:

$$m(T) = \tfrac{1}{4}((a + (b + c))(a + (b - c))(c + (a - b))(c - (a - b)))^{1/2}, \tag{103}$$

where a, b and c denote the lengths of the edges of triangle T after they have been ordered to satisfy

$$c \leqslant b \leqslant a. \tag{104}$$

Table 1
Computational efficiency of the boundary condition (8), applied on Σ being a circle or a square, in the case of a square-shaped fibre and $\lambda/h = 50$

Boundary condition (8) associated with	Σ	l	Number of unknowns of GEVP
Eq. (9)	Circle	1	14,763
Eq. (9)	Square	1	9499
Eq. (10)	Circle	1/2	5249
Eq. (10)	Square	1/2	3367

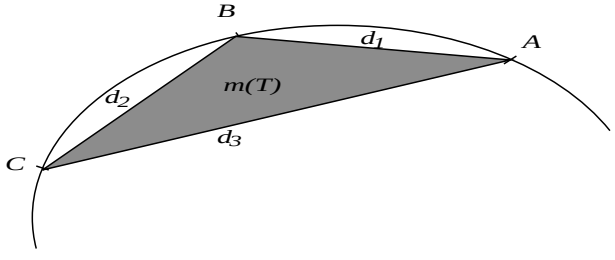

Fig. 3. Computation of the curvature at a given point.

Given that, solving the variational problem (11) and (12) consists in solving the following quadratic eigenvalue problem

$$\text{(QEVP)} \quad \text{Find } \lambda_\Sigma^h \in]0, V^2[\text{ and } x \in \mathbb{R}^N;\ x \neq 0 \text{ such that } Ax + \lambda_\Sigma^h Bx + \sqrt{\lambda_\Sigma^h} C \quad x = 0, \tag{105}$$

where λ_Σ^h is an approximation of λ_Σ and x is an eigenvector associated to λ_Σ^h. N is the number of degrees of freedom (dof). A, B and C are symmetric matrices. A is the sum of a stiffness – and a mass-like matrices. B is a mass matrix. B is then positive definite. C is a mass-type matrix defined on Σ. It is crucial to observe that the matrix C is sparse (quasi-tridiagonal), because of the local characteristic of the artificial boundary condition. In addition, the finite element approximation of the integral containing the curvature $\mathscr{K}$ in Eq. (89) introduces an additional mass-like matrix on Σ to be added to the matrix A.

In order to solve numerically QEVP, we introduce the following generalized eigenvalue problem GEVP

$$\text{(GEVP)} \quad \text{Find } \mu_\Sigma^h \in]0, V^2[\text{ and } z \in \mathbb{R}^{2N};\ z \neq 0 \text{ such that } \widetilde{A} z = \mu_\Sigma^h \widetilde{B} z, \tag{106}$$

where

$$\widetilde{A} = \begin{bmatrix} -C & -B \\ A & 0 \end{bmatrix} \tag{107}$$

and

$$\widetilde{B} = \begin{bmatrix} B & 0 \\ 0 & B \end{bmatrix}. \tag{108}$$

It is easy to verify that GEVP and QEVP are equivalent in the following sense:

(i) If the couple (λ_Σ^h, x) is a solution of QEVP, then the couple (μ_Σ^h, z), defined by

$$\mu_\Sigma^h = \sqrt{\lambda_\Sigma^h} \tag{109}$$

and

$$z = \begin{bmatrix} x \\ y \end{bmatrix} \tag{110}$$

with

$$y = \frac{1}{\sqrt{\lambda_\Sigma^h}} B^{-1} A x \tag{111}$$

is a solution of GEVP.

(ii) Conversely, if the couple (μ_Σ^h, z) is a solution of GEVP, then the couple (λ_Σ^h, x) defined by $\lambda_\Sigma^h = (\mu_\Sigma^h)^2$ and x is the first N components of the vector z, is a solution of QEVP.

Therefore, in order to compute (λ_Σ^h, x) solution of QEVP, we first compute the couple (μ_Σ^h, z) solution of GEVP using any preferred eigenvalue algorithm. Then, we deduce the couple (λ_Σ^h, x) from (ii).

In this paper, we compute the solutions of GEVP by means of the so-called *Implicitly Restarted Arnoldi Method IRAM* [15]. It is an iterative algorithm of *QR*-type [23,31]. The application of this method requires solving – at each iteration – a non-symmetric linear system. We have performed such computations using the *Generalized Minimal Residual method GMRES* [24].

5.2. Accuracy and performance evaluation

The objective here is to demonstrate by several computational examples that using the boundary condition (8) associated with Eq. (10) applied on an artificial boundary Σ that is parallel to the interface core–cladding of the considered fibre, rather than condition (8) associated with Eq. (9) applied on Σ being a circle as suggested in [11], improves the computational efficiency while maintaining the same level of accuracy.

We point out that we will not perform a grid convergence study in this paper to address the effect of the discretization. This issue has been already investigated in details in [11]. Therefore, we have first considered the simple case of a step-index circular-shaped fibre of radius a. This case is simple in the sense that the dispersion curves of the guided modes, solutions of EVP can be computed analytically [18,20,25,30]. Hence, this case is interesting because it is possible to investigate analytically, i.e., in the absence of errors due to the finite element discretization, the performance of each boundary condition [see Eqs. (8), (9) and (8), (10)], when Σ is chosen to be a circle. The numerical results reported in Appendix A indicate clearly, as expected from the analysis therein, the superiority of the boundary condition of order 1 [see Eqs. (8) and (10)] over the boundary condition of order 1/2 [see Eqs. (8) and (9)]. Indeed, it has been shown in Appendix A that, to compute the propagation constants with a relative error less than 1%, the use of condition (10) rather than condition (9), reduces the size of the computational domain by – at least – a factor 2.

In the second set of numerical experiments that we have performed, we considered only the class of step-index optical fibres. We have computed the dispersion curves of (a) a square-shaped fibre, and (b) an optical coupler which core is made up of two separate disks. In these experiments, we have computed the dispersion curves by solving the generalized eigenvalue problem GEVP, for each proposed boundary condition [see Eqs. (8), (9) and Eqs. (8), (10)] and for an artificial boundary Σ which shape is (a) circular, and (b) parallel to the interface core–cladding of the considered structure. The objective here is to assess, for a prescribed level of accuracy, the computational efficiency for each choice of the shape of Σ and the boundary conditions (8), (9) and (8), (10).

Before we present the obtained numerical results for each fibre, we introduce the following classical notation:

$$\widetilde{V} = ka\sqrt{n_+^2 - n_\infty^2}, \tag{112}$$

$$b_\Sigma^h = \frac{\lambda_\Sigma^h}{k^2\left(n_+^2 - n_\infty^2\right)}, \tag{113}$$

where a is a dimension that characterizes the core of the considered optical fibre. $\widetilde{V}$ is called the normalized frequency and b_Σ^h is the numerical normalized propagation constant. Hence, we have $0 < b_\Sigma^h < 1$.

We also point out that in all performed numerical experiments, we have set

$$n_+ - n_\infty = 0.01 \tag{114}$$

so that the weak guidance conditions are satisfied [18,25,30].

5.2.1. Case of a square-shaped fibre

We consider here the case of an optical fibre which core is a square centered at the origin and with a side's length equals to $a = 0.4$ μm. The artificial boundary Σ is chosen to be either a circle or a square surrounding the core of the fibre as depicted in Fig. 4. The resulting computational domain Ω_Σ is discretized with a mesh resolution $\lambda/h = 50$. We have then computed the dispersion curves of the first five guided modes and compared the obtained results to those computed analytically and reported in [18].

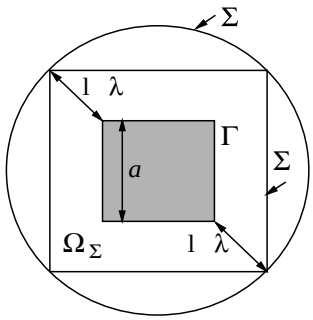

Fig. 4. Computational domain for a square-shaped optical fibre. Circular-shaped versus square-shaped artificial boundary Σ.

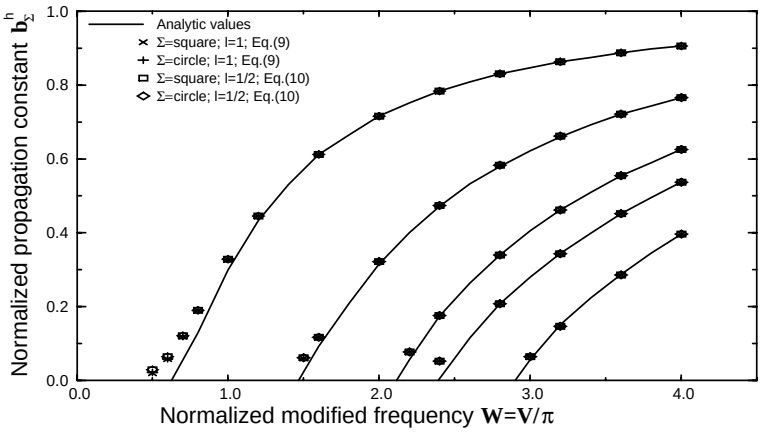

Fig. 5. Dispersion curves of the first five guided modes of a square-shaped optical fibre.

We observe that for values of $\widetilde{V}$ that are far from the cut-off frequencies, the dispersion curves depicted in Fig. 5 are computed with a relative error less than 1% when (a) condition (8) and (9) is applied on Σ (a circle or a square) located – at least – at one wavelength from the corners of the interface core–cladding, i.e., $l = 1$ (see Fig. 7), and (b) condition (8) and (10) is applied on Σ (a circle or a square) for $l = 1/2$. Moreover, the results reported in Table 1 indicate that the use of condition (8) and (10) (or even condition (8) and (9)) applied on Σ being a square rather than a circle reduces the number of unknowns of GEVP by about 36%. Furthermore, using condition (8) and (10) applied on Σ being a square rather than condition (8) and (9) applied on a circle as suggested in [11], reduces the size of GEVP by a factor 4.4 while preserving the level of accuracy Fig. 6.

5.2.2. Case of an optical coupler

The optical coupler we consider here is an optical fibre with two circular-shaped cores. The artificial boundary Σ that surrounds the cores is chosen to be either a circle or a *cigar* as illustrated in Fig. 7.

We assess here the computational efficiency of condition (8) by computing only the fundamental mode that is propagating in the considered structure. The normalized frequency is fixed at $\widetilde{V} = 2$, i.e., we consider the monomode regime, and the computational domain Ω_Σ is discretized using 20 linear elements per wavelength. We have computed the propagation constants of the odd and even fundamental modes [18] by

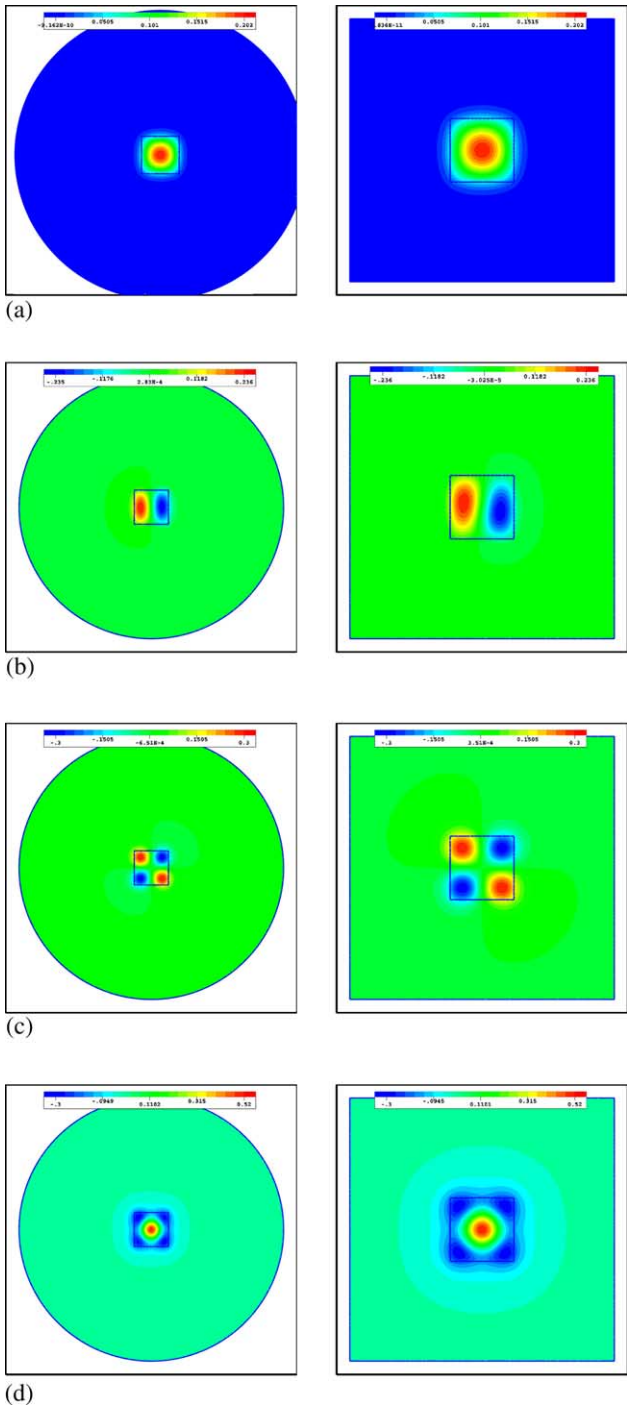

Fig. 6. Isovalues of the first four guided modes computed in the case of a square-shaped fibre, for $\lambda/h = 50$. Left column: Eq. (9); $\Sigma = circle$; $l = 1$. Right column: Eq. (10); $\Sigma = square$; $l = 1/2$. (a) Mode $E_{11}^{x,y}$. (b) Mode $[E_{12}^{x,y}, E_{21}^{x,y}]$. (c) Mode $E_{22}^{x,y}$ and (d) Mode $[E_{13}^{x,y}, E_{31}^{x,y}]$.

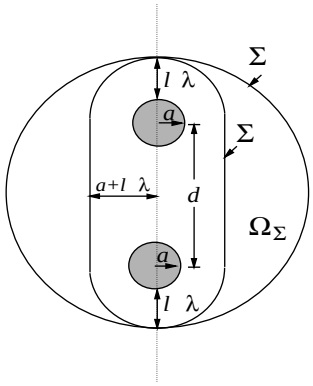

Fig. 7. Computational domain for an optical coupler. Cigar-shaped versus circular-shaped artificial boundary Σ.

Table 2
Computational efficiency of the boundary condition (8), applied on Σ being a circle or a cigar, for three selected coupling distances d, and for $\lambda/h = 20$

Boundary condition (8) associated with	Σ	l	Number of unknowns $d/a = 2$	Number of unknowns $d/a = 3$	Number of unknowns $d/a = 6$
Eq. (9)	Circle	1	4312	5125	8485
Eq. (9)	Cigar	1	3620	4066	5297
Eq. (10)	Circle	1/2	2103	2693	4984
Eq. (10)	Cigar	1/2	1627	1904	2684

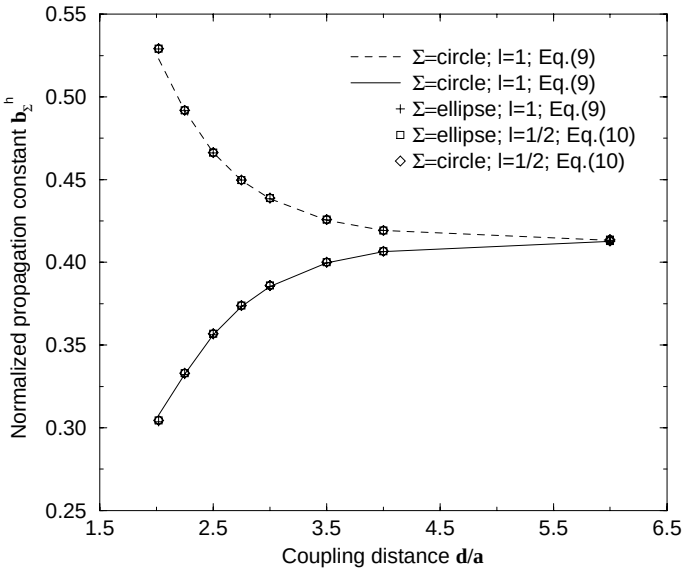

Fig. 8. Sensitivity of the propagation constant of the fundamental mode to the coupling distance d/a. The continuous line is for the odd mode whereas the dashed line stands for the even mode.

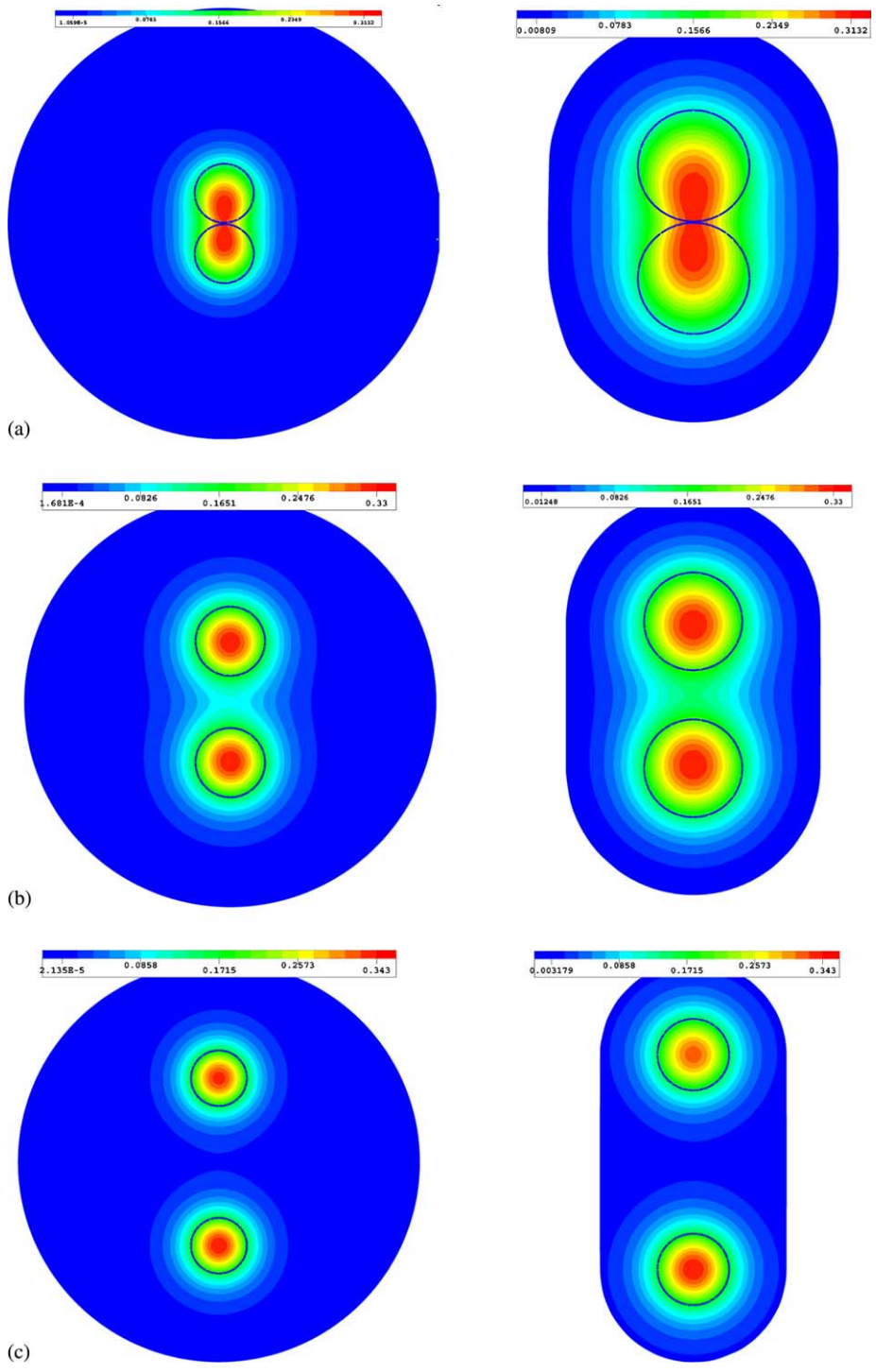

Fig. 9. Dependence of the computed isovalues of the fundamental *even* mode of an optical fiber on the coupling distance d/a, for $\lambda/h = 20$. Left column: Eq. (9); $\Sigma = circle$; $l = 1$. Right column: Eq. (10); $\Sigma = cigar$; $l = 1/2$. (a) $d/a = 2$, (b) $d/a = 3$ and (c) $d/a = 6$.

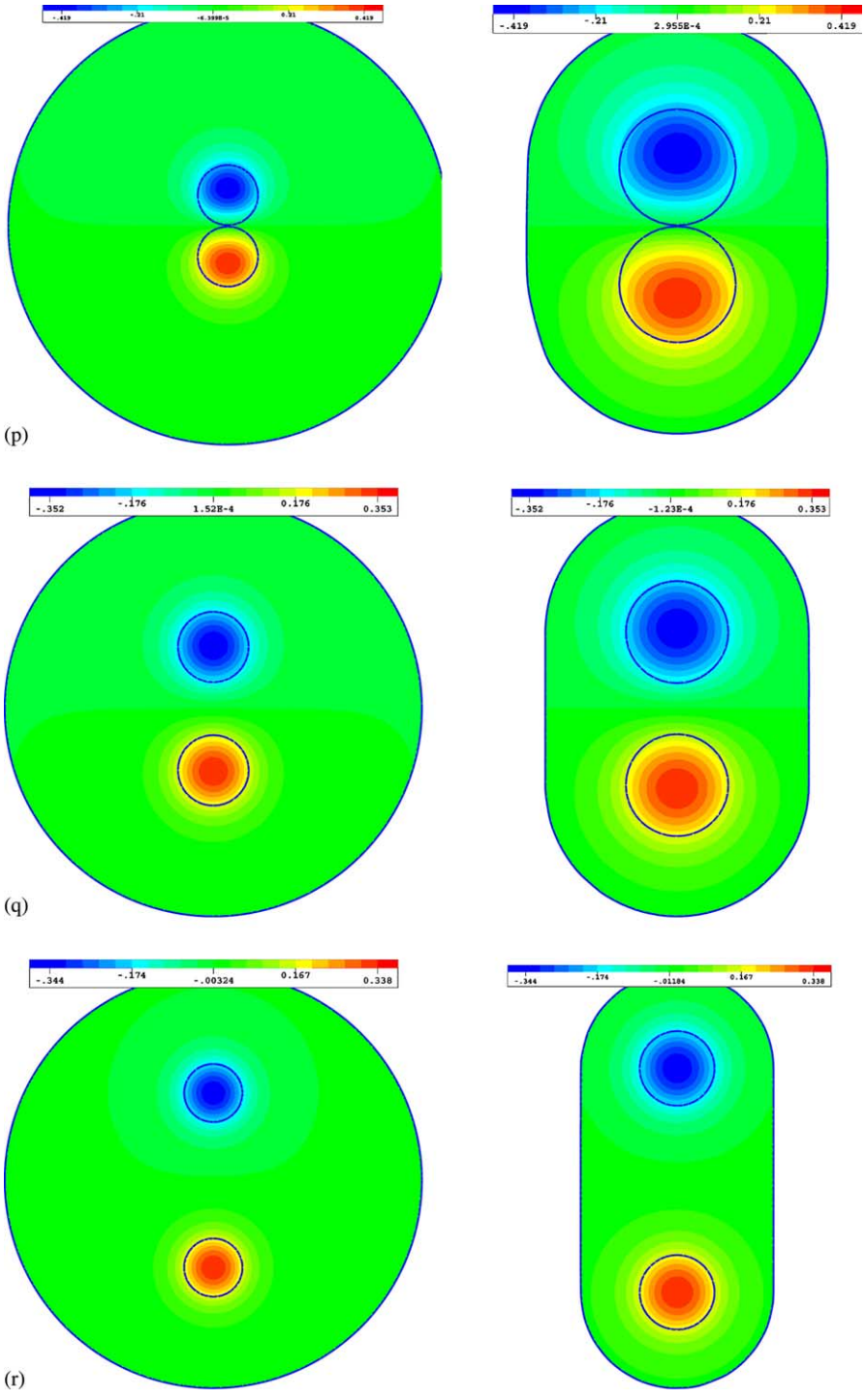

Fig. 10. Dependence of the computed isovalues of the fundamental *odd* mode of an optical fiber on the coupling distance d/a, for $\lambda/h = 20$. Left column: Eq. (9); $\Sigma = circle$; $l = 1$. Right column: Eq. (10); $\Sigma = cigar$; $l = 1/2$. (p) $d/a = 2$, (q) $d/a = 3$ and (r) $d/a = 6$.

varying the coupling distance d/a in the interval $[2.0, 6.0]$. The obtained results are reported in Table 2 and Figs. 8–10. It is important to recall here (see [11]) that the results obtained by using condition (8) associated with Eq. (9) applied on a circle located at one wavelength from either one of the two cores (see Fig. 7) are in perfect agreement with those obtained by an integral method [5] (with a relative error less than 1%).

We can make here the following two observations:

- both conditions (8), (9) and (8), (10) deliver results with a comparable accuracy regardless of the choice of the geometry of the exterior boundary Σ. However, the results obtained with condition (8) and (10) require that Σ is located at half wavelength from the interface core–cladding (see Fig. 7) while Σ needs to be at least at one wavelength from the same interface for condition (8) and (9).
- The results reported in Table 2 indicate clearly that using condition (8) and (10) applied on a cigar-shaped exterior boundary rather than condition (8) and (9) applied on a circle reduces the number of unknowns in GEVP by a factor ranging from 2.5 to 3.2, depending on the value of the coupling distance d/a. More specifically, for $d/a = 2$, i.e., in the case of a "strong" coupling, the factor of reduction is about 2.5, for $d/a = 3$, i.e., for a "mild" coupling, the factor of reduction is equal to 2.7, and for $d/a = 6$, i.e., a "weak" coupling, the factor of reduction is about 3.2.

6. Summary and conclusion

By approximating the D_tN operator using the micro-local analysis, we have derived exterior boundary conditions to reduce the eigenvalue problem EVP, that characterizes the propagation of guided waves in optical structures, to the generalized eigenvalue problem BVP set in a bounded domain.

Unlike the condition suggested in [11] which can operate only on circular-shaped fictitious boundaries, the suggested conditions can be applied on arbitrarily shaped but convex exterior boundaries. Hence, these new conditions allow the utilization of artificial boundaries that circumscribe more closely the interface core–cladding of the considered optical waveguide than the circular boundaries, and therefore, improve significantly the computational efficiency of the finite element solution of the obtained generalized eigenvalue problem GEVP. Indeed, the numerical results reported in this paper, indicate that condition (8) and (10) reduces the number of GEVPs unknowns by a factor ranging between two and six, depending on the geometry of the optical waveguide, while maintaining the level of accuracy.

Acknowledgements

Part of this research was carried out while the third author was visiting the Université de Pau et des Pays de l'Adour. The hospitality and the support are gratefully acknowledged.

Appendix A. Case of a step-index circular-shaped fibre: analytical study

Our aim here is to demonstrate analytically that using the boundary condition (8) associated with Eq. (10) rather than Eq. (9) can improve significantly the computational efficiency by reducing the size of the computational domain.

To accomplish such analysis, we consider the particular case of a step-index optical fibre with a circular-shaped core of radius equals to 1, surrounded by an artificial boundary Σ chosen to be a circle of radius $R > 1$ (see Fig. 11). The obtained computational domain Ω_Σ is then a disk of radius R.

Then, the use of polar coordinates allows to prove that the propagation constants solutions of BVP can be characterized as solutions of a dispersion equation. Therefore, we are able to compute the dispersion

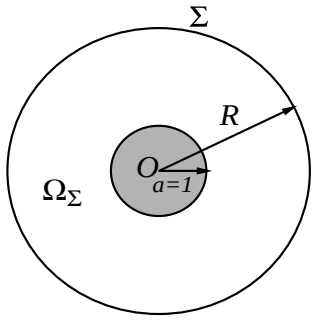

Fig. 11. A step-index circular-shaped optical fiber, with a circular-shaped artificial boundary Σ.

curves of the guided modes and evaluate the accuracy of the obtained results in the absence of finite element disretization errors.

To do this, we first introduce the following convenient notations:

$$\lambda_{1,R}^2 = (1 - b_R)\widetilde{V}^2 \quad \text{and} \quad \lambda_{2,R}^2 = -b_R\widetilde{V}^2, \tag{A.1}$$

$$\lambda_{j,R} = \sqrt{\left|\lambda_{2,R}^2\right|}; \quad j = 1, 2, \tag{A.2}$$

where $\widetilde{V}$ is the normalized frequency and b_R is the normalized propagation constant solution of BVP.

- J_v (resp., H_v^1) is Bessel (resp., Hankel) function of first kind; $v \in \mathbb{N}$ [1]
- K_v and I_v are the modified Bessel functions of the first kind [1].

We are now ready to establish one of the main results of this appendix.

Lemma A.1. *The normalized eigenvalues b_R solutions of BVP satisfy the following alternative (DE) either*

$$\lambda_{1,R}\frac{J_{v+1}(\lambda_{1,R})}{J_v(\lambda_{1,R})} = \lambda_{2,R}\frac{K_{v+1}(\lambda_{2,R})}{K_v(\lambda_{2,R})}\left[\frac{1 + C(R,v)\frac{I_{v+1}(\lambda_{2,R})}{K_{v+1}(\lambda_{2,R})}}{1 - C(R,v)\frac{I_v(\lambda_{2,R})}{K_v(\lambda_{2,R})}}\right], \tag{A.3}$$

$$\textit{if } K_v(\lambda_{2,R}) - C(R,v)I_v(\lambda_{2,R}) \neq 0 \tag{A.4}$$

or

$$J_v(\lambda_{1,R}) = 0 \quad \textit{if condition (A.4) is not satisfied} \tag{A.5}$$

where

$$C(R,v) = \frac{\lambda_{2,R}K_v'(\lambda_{2,R}R) + \left\{\lambda_{2,R} + \frac{1}{2R}\right\}K_v(\lambda_{2,R}R)}{\lambda_{2,R}I_v'(\lambda_{2,R}R) + \left\{\lambda_{2,R} + \frac{1}{2R}\right\}I_v(\lambda_{2,R}R)}. \tag{A.6}$$

Proof of Lemma A.1. We prove this result in four steps.

Step 1. We adopt the following representation in polar coordinates of the eigenvector u_R associated to the eigenvalue b_R, solution of BVP.

$$u_R(x) = \widetilde{u}_R(r)\mathrm{e}^{\mathrm{i}v\theta}; \ r > 0, \ \theta \in [0, 2\pi[\text{ and } v \in \mathbb{N}, \tag{A.7}$$

Step 2. One can easily verify that $\widetilde{u}_R$ is of the form

$$\widetilde{u}_R(r) = \begin{cases} A_v J_v(\lambda_{1,R} r), & 0 < r < 1, \\ B_v K_v(\lambda_{2,R} r) + C_v I_v(\lambda_{2,R} r), & 1 < r < R, \end{cases} \tag{A.8}$$

where A_v, B_v, and C_v are three constants depending on v and R, that are determined from the artificial boundary condition (8) associated with Eq. (10) and the transmission conditions at the interface core–cladding of the considered fibre.

Step 3. We rewrite the condition (8) associated with Eq. (10) in polar coordinates as follows.

$$\frac{\mathrm{d}\widetilde{u}_R}{\mathrm{d}r} + \lambda_{2,R}\widetilde{u}_R + \frac{1}{2R}\widetilde{u}_R = 0; \quad r = R. \tag{A.9}$$

From Eqs. (A.8) and (A.9), we deduce that

$$\begin{aligned} &B_v\lambda_{2,R}K_v'(\lambda_{2,R}R) + C_v\lambda_{2,R}I_v'(\lambda_{2,R}R) + B_v\lambda_{2,R}K_v(\lambda_{2,R}R) + C_v\lambda_{2,R}I_v(\lambda_{2,R}R) \\ &\quad + \frac{1}{2R}B_vK_v(\lambda_{2,R}R) + \frac{1}{2R}C_vI_v(\lambda_{2,R}R) = 0. \end{aligned} \tag{A.10}$$

Moreover, we have

$$\frac{1}{2R}I_v(\lambda_{2,R}R) + \lambda_{2,R}\left\{I_v'(\lambda_{2,R}R) + I_v(\lambda_{2,R}R)\right\} > 0; \quad v \in \mathbb{N}. \tag{A.11}$$

Therefore, we deduce that

$$C_v = -C(R,v)B_v, \tag{A.12}$$

where $C(R,v)$ is given by Eq. (A.6).

Step 4. We apply now the transmission conditions to the field $\widetilde{u}_R$ given by Eq. (A.8) and deduce that

$$A_vJ_v(\lambda_{1,R}) = B_v(K_v(\lambda_{2,R}) - C(R,v)I_v(\lambda_{2,R})) \tag{A.13}$$

and

$$A_v\lambda_{1,R}J_v'(\lambda_{1,R}) = B_v\lambda_{2,R}\left(K_v'(\lambda_{2,R}) - C(R,v)I_v'(\lambda_{2,R})\right). \tag{A.14}$$

Therefore, the dispersion equation *DE* is an immediate consequence of Eqs. (A.13) and (A.14). □

Remark A.1. We recall (see [11]) that the dispersion equation corresponding to BVP in the case of the boundary condition associated with Eq. (9), is similar to DE with

$$C(R,v) = \frac{K_v'(\lambda_{2,R}R) + K_v(\lambda_{2,R}R)}{I_v'(\lambda_{2,R}R) + I_v(\lambda_{2,R}R)}; \quad \text{for Sommerfeld b.c. of order } 1/2. \tag{A.15}$$

Since the dispersion equation corresponding to *EVP* is similar to *DE* with $C(R,v) = 0$, one needs to analyze the asymptotic behavior of $C(R,v)$ when R tends to $+\infty$. In order to do this, we note from now and on $C(R,v) = C_1(R,v)$ when we refer to Eq. (A.6) and $C(R,v) = C_{1/2}(R,v)$ when we refer to Eq. (A.15). We observe that the subscript stands for the order of the corresponding condition.

Lemma A.2. *For v fixed, we have the following asymptotic behavior when R tends to infinity*

$$C_1(R,v) \sim \pi\frac{4v^2-1}{32\lambda_{2,R}^2R^2}\mathrm{e}^{-2\lambda_{2,R}R}. \tag{A.16}$$

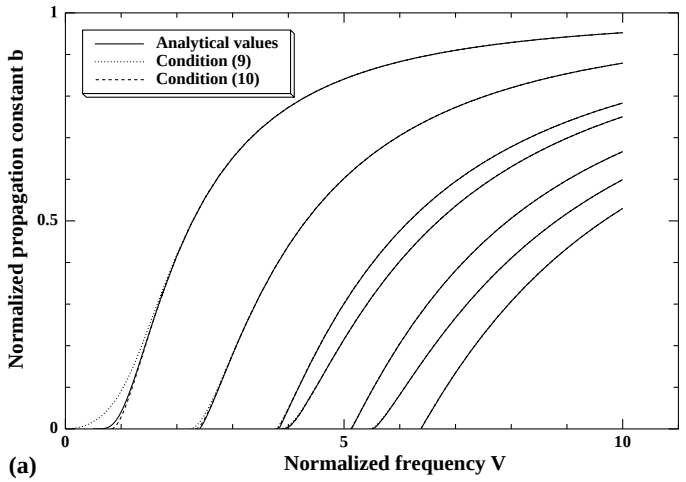

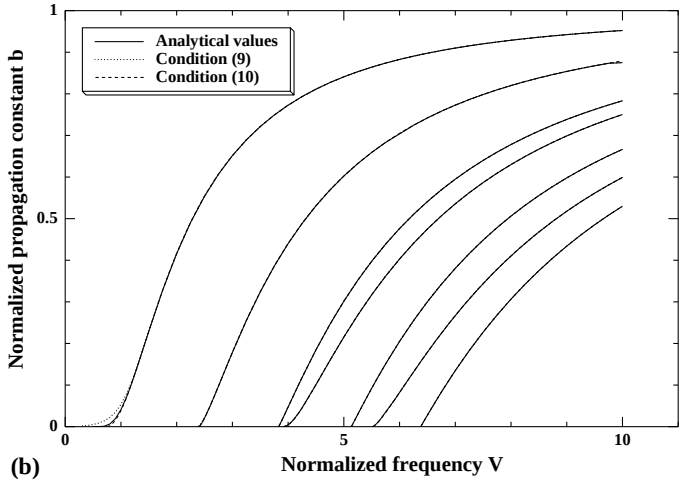

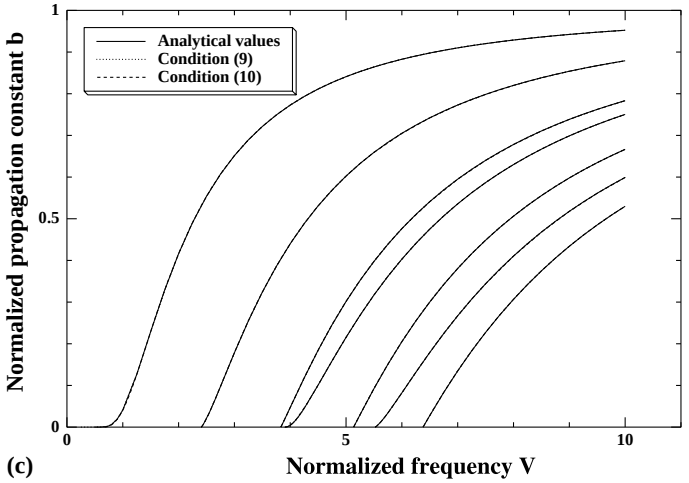

Fig. 12. Comparison of the dispersion curves for three different values of R. (a) $R = 2$, (b) $R = 4$ and (c) $R = 10$.

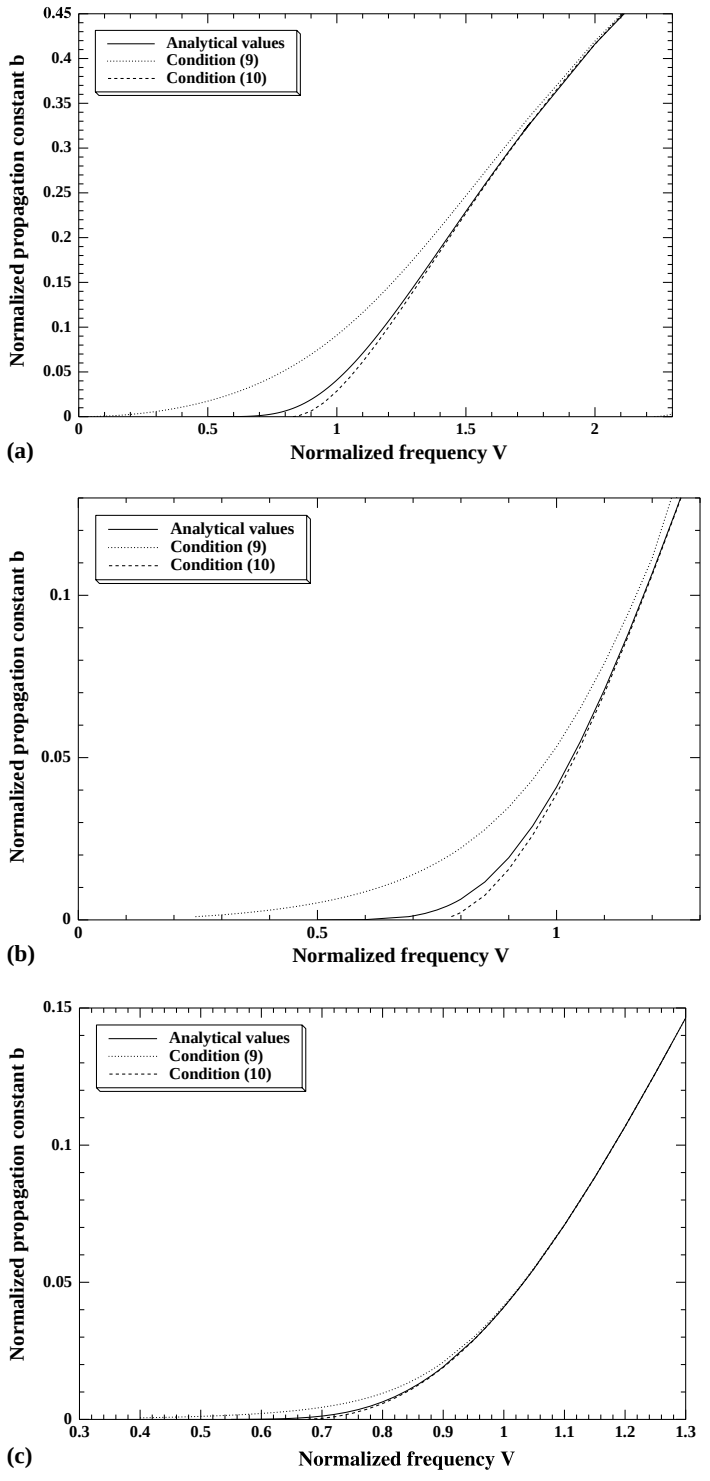

Fig. 13. Zoom around the cut-off frequency of the fundamental mode LP_{01}. (a) $R = 2$, (b) $R = 4$ and (c) $R = 10$.

Proof of Lemma A.2. Eqs. (9.7.2) and (9.7.4) in [1] imply that

$$\lambda_{2,R}K_\nu'(\lambda_{2,R}R)+\left\{\lambda_{2,R}+\frac{1}{2R}\right\}K_\nu(\lambda_{2,R}R)\sim\frac{4\nu^2-1}{16\lambda_{2,R}R^2}\sqrt{\frac{\pi}{2\lambda_{2,R}R}}\mathrm{e}^{-\lambda_{2,R}R}. \tag{A.17}$$

Similarly, Eqs. (9.7.1) and (9.7.3) in the same [1] give

$$\lambda_{2,R}I_\nu'(\lambda_{2,R}R)+\left\{\lambda_{2,R}+\frac{1}{2R}\right\}I_\nu(\lambda_{2,R}R)\sim\frac{2\lambda_{2,R}}{\sqrt{2\pi\lambda_{2,R}R}}\mathrm{e}^{\lambda_{2,R}R} \tag{A.18}$$

Eq. (A.16) is therefore deduced from Eqs. (A.6), (A.17) and (A.18). □

Remark A.2. From the asymptotic behavior of $C_1(R,\nu)$ given by Eq. (A.16), we deduce that the dispersion equation *DE* converges to the exact solution as $1/R^2$. On the other hand, it has been shown in [11] that in the case of condition (8) and (9), the convergence is as $1/R$. Therefore, this result proves that condition (8) and (10) has the potential for reducing the size of the computational domain Ω_Σ.

A.1. Numerical illustrations

The objective here is to demonstrate numerically that the use of condition (8) and (10) requires a computational domain Ω_Σ smaller than the one needed for condition (8) and (9), for a prescribed accuracy. For this purpose, we have computed, for different values of the radius R, which characterizes the size of the computational domain, the dispersion curves of the first seven guided modes for both conditions (8) and (9) and (8) and (10) and compared them to those obtained analytically [18]. This numerical investigation allows to make the following two observations

- First, from the results reported in Fig. 12, we deduce that, for values of $\widetilde{V}$ far from the cut-off frequencies, both conditions have a comparable performance for computing the propagation constants.
- Second, in the neighborhood of the cut-off frequencies, condition (8) and (10) delivers results with a better accuracy than those obtained using condition (8) and (9), as it is clearly illustrated in Fig. 13 in the case of the fundamental mode. Condition (8) and (9) requires a much larger computational domain to reach the level of accuracy delivered by condition (8) and (10) as illustrated in Figs. 12(b) and (c).

References

[1] A. Abramowitz, I.A. Stugun, Handbook of Mathematical Functions, Dover, New York, 1964.
[2] X. Antoine, H. Barucq, A. Bendali, Bayliss–Turkel-like radiation conditions on surfaces of arbitrary shape, J. Math. Anal. Appl. 229 (1999) 184–211.
[3] H. Barucq, R. Djellouli, Développement de conditions aux limites locales pour le calcul par éléments finis des modes guidés dans les fibres optiques, Partie I: Analyse mathématique, Rapport Interne 00-13, LMA ERS2055, PAU, France, 2000.
[4] A. Bayliss, M. Gunzburger, E. Turkel, Boundary conditions for the numerical solution of elliptic equations in exterior regions, SIAM J. Appl. Math. 42 (1982) 430–451.
[5] C. Bekkey, R. Djellouli, An integral method to compute guided modes of an optical fiber in the vectorial case, Appl. Math. Model. 24 (2000) 697–713.
[6] A.S. Bonnet, R. Djellouli, Etude mathématique des modes guidés d'une fibre optique. Résultats élémentaires et extension au cas de couplage. Rapport interne CMAP, 182, Ecole Polytechnique, France, 1988.
[7] A.S. Bonnet-Bendhia, N. Gmati, Spectral approximation of a boundary condition for an eigenvalue problem, SIAM J. Numer. Anal. 32 (1995) 1263–1279.
[8] A.S.B. Bonnet, R. Djellouli, High-frequency asymptotic of guided modes in optical fibres, IMA J. Appl. Math. 52 (1994) 271–287.
[9] J. Chazarain, A. Piriou, Introduction to the Linear Partial Differential Equations, North-Holland, 1982.
[10] R. Courant, D. Hilbert, Methods of Mathematical Physics, Interscience, 1962.

[11] R. Djellouli, C. Bekkey, A. Choutri, H. Rezgui, A local boundary condition coupled to a finite element method to compute guided modes of optical fibres under the weak guidance assumptions, J. Math. Meth. Appl. Sci. 23 (2000) 1551–1583.
[12] M.P. Do Carmo, Differential Geometry of Curves and Surfaces, Prentice-Hall, New Jersey, 1976.
[13] D. Givoli, Non-reflecting boundary conditions. A review article, J. Comput. Phys. 94 (1991) 1–29.
[14] T. Hagstrom, Radiation boundary conditions for the numerical simulation of waves, Acta Numer. (1999) 47–106.
[15] R.B. Lehoucq, D.C. Sorensen, C. Yang, ARPACK Users guide: Solutions for large scale eigenvalue problems by implicitly restarted Arnoldi methods. Draft, July 31st 1996. ftp address: ftp.caam.rice.edu.
[16] N. Mabaya, P.E. Lagasse, P. Vandenbulcke, Finite element analysis of optical waveguides, IEEE Trans. Microwave Theor. Tech. 29 (1981) 600–605.
[17] A. Majda, S. Osher, Reflection of singularities at the boundary, Comm. Pure Appl. Math. 28 (1975) 479–499.
[18] D. Marcuse, Theory of Dielectric Optical Waveguides, Academic Press, New York, 1974.
[19] L. Nirenberg, Pseudodifferential operators and some applications, Lectures on Linear Partial Differential Equations, CBMS Regional Conf. Math. 17 (1973) 19–58.
[20] J.P. Pocholle, Propagation dans les fibres optiques monomodes, Revue technique de Thomson-CSF, 15, 1983.
[21] P.A. Raviart, J.M. Thomas, Introduction à l'analyse numérique des équations aux dérivées Partielles, Masson, Paris, 1983.
[22] M. Reed, B. Simon, in: Methods of Modern Mathematical Physics, vol. 2, Academic Press, New York, 1978.
[23] Y. Saad, Numerical Methods for Large Eigenvalue Problems, Manchester University Press, New York, 1992.
[24] Y. Saad, M.H. Schultz, A generalized minimal residual algorithm for solving nonsymmetric linear systems. Research Report yaleu/dcs/rr-254, Department of Computer Science, Yale University, 1983.
[25] A.W. Snyder, J.D. Love, Optical Waveguide Theory, Chapman & Hall, London, 1983.
[26] M. Spivak, A Comprehensive Introduction to Differential Geometry, Publish or Perish, 1979.
[27] M.E. Taylor, Pseudodifferential Operators, Princeton University Press, Princeton, NJ, 1981.
[28] F. Treves, Pseudodifferential and Fourier Integral Operators, in: J.J. Kohn (Ed.), The University Series in Mathematics, vol. 1, Plenum Press, New York, 1980.
[29] S. Tsynkov, Numerical solutions of problems in unbounded domains. A review article, Appl. Numer. Math. 27 (1998) 465–532.
[30] C. Vassalo, Théorie des Guides D'ondes Electromagnétiques, Tomes 1 & 2. Eyrolls et CNET-ENST, Paris, 1985.
[31] J.H. Wilkinson, The Algebraic Eigenvalue Problem, Clarendon Press, Oxford, UK, 1965.
[32] C. Yeh, K. Ha, S.B. Dong, W.P. Brown, Single mode optical waveguides, Appl. Opt. 18 (1979) 1490–1504.